Plasmon-Enhanced Optothermal Manipulation

Zhihan Chen, Jingang Li, and Yuebing Zheng

Abstract Plasmon-enhanced optical heating can synergize optics and thermal fields to offer a versatile platform for optothermal manipulation of colloidal particles and living cells. By exploiting entropically favorable photon-phonon conversion and universal heat-directed migration, various optothermal tweezing techniques have been developed. Under the thermal gradient field enabled by plasmonic heating, opto-thermophoretic tweezers harness the permittivity gradient at particle-solvent interfaces to direct particles and cells toward the plasmonic hotspot via thermophoresis. Opto-thermoelectric tweezers can manipulate charged colloidal particles with various sizes, materials, and shapes in a localized electric field that is generated by the plasmon-enhanced electrolyte Seebeck effect. In addition, conventional plasmonic trapping can be significantly improved by three types of plasmon-enhanced optothermal-hydrodynamics, *i.e.*, thermo-plasmonic convection, Marangoni convection, and electrothermoplasmonic flow. These plasmon-enhanced optothermal convective flows can rapidly transport or concentrate free-dispersed objects to the plasmonic nanostructures, which significantly enhance the trapping efficiency of micro-and nano-objects. With their low operational power, simple optics, and wide applicability, plasmon-enhanced optothermal manipulation techniques can be applied to optothermal assembly of colloidal matter, non-invasive manipulation of cells and biological objects, and *in-situ* characterization of optical coupling in colloidal superstructures for a wide range of applications in photonics, materials science, colloidal science, biology, and medical engineering.

Z. Chen · J. Li

Materials Science & Engineering Program and Texas Materials Institute, The University of Texas at Austin, Austin, TX, USA

Y. Zheng (✉)

Materials Science & Engineering Program and Texas Materials Institute, The University of Texas at Austin, Austin, TX, USA

Walker Department of Mechanical Engineering, The University of Texas at Austin, Austin, TX, USA
e-mail: zheng@austin.utexas.edu

1 Introduction

Since Ashkin and co-workers first proposed to exploit light to manipulate micro-and nano-objects in 1986 [1], optical tweezers have been developed rapidly in the last 35 years and were awarded the Nobel Prize in Physics in 2018. Conventional optical tweezers can trap biological objects, plasmonic particles, and various dielectric particles in both two-dimensional (2D) and three-dimensional (3D) spaces [2–8]. However, trapping subwavelength objects via optical tweezers is challenging due to the diffraction limit of the incident light [9], which stimulated the development of plasmonic tweezers to overcome this limitation [10–15]. In brief, plasmonic tweezers rely on the interaction between incident light and plasmonic nanostructures consisting of noble metals [16–19] (or titanium nitride [20], graphene [21, 22], etc.) to trigger local near-field enhancement and strong gradient forces to trap nano-objects beyond the diffraction limit. However, the inherent Joule heating of metallic nanostructures upon laser irradiation in plasmonic tweezers sometimes leads to the failure of stable trapping or even thermal damages to the target objects [23, 24] because of the undesired thermophoresis, heat-induced convection, and/or the high temperature at the surface.

Apart from preventing heat generation or dissipating the heat via materials or structural designs [11, 25, 26], more strategies were proposed to reversely take advantage of the plasmonic heating to improve the manipulation efficiency of plasmonic tweezers [27, 28]. For instance, as the plasmonic heating occurs, a temperature gradient field is established in the vicinity of the plasmonic nanostructure, where the thermophoretic motions of suspended objects along or against the temperature gradient can be exploited for particle trapping and manipulation [29, 30]. In an ionic solution, differentiated thermophoretic motions of cations and anions can further facilitate the formation of thermoelectric fields to enabling opto-thermoelectric trapping of charged objects [31]. With an increasing irradiation intensity or illumination area, two types of optothermal flows, namely thermo-plasmonic and Marangoni convective flow, can take effect to deliver distant suspended particles towards the irradiated nanostructures, improving the trapping efficiency of plasmonic tweezers at low particle concentrations [32]. Moreover, local plasmonic heating also triggers a gradient of permittivity and electrical conductivity of the heated fluid. By applying an external a.c. electric field, the electrothermoplasmonic (ETP) flow is established and can be exploited for effective nano-object manipulation [33].

In this chapter, we first introduce the mechanism of plasmonic heating and feature several representative plasmonic heating substrates. Subsequently, plasmon-enhanced optothermal trapping and tweezing based on thermophoresis, thermo-

electricity, and thermo-plasmonic/Marangoni/ETP convective flows are discussed, respectively, including their working principles and applications. Finally, we give the summary and outlook of the plasmon-enhanced photothermal trapping and tweezing.

2   Plasmonic Photothermal Effect

Plasmonic photothermal effect is commonly initiated by the photoexcitation of metallic nanostructures [34]. When electromagnetic waves irradiate the metallic nanostructures with proper wavelength(s), the conduction electrons in the metal can oscillate collectively, known as localized surface plasmon resonance (LSPR). LSPR then leads to an intense electromagnetic field on the nanostructure surface, which can decay radiatively and non-radiatively. Specifically, radiative decay induces reemission of light, while non-radiative decay can be achieved via electron-electron collisions or electron-lattice phonon coupling, resulting in light-to-heat conversion (Fig. 1). Note that the heating of metallic nanostructures based on light irradiation can be quantitatively described by a value called absorption cross-section, $C_{abs} = Q/I$, where Q is the heat generated by the plasmonic nanostructure and I represents the intensity of incident light. Since the plasmonic photothermal effect relies on the coupling between light and electronic oscillations of metallic nanostructures, C_{abs} is a function of the shape and composition of plasmonic nanostructures and can also vary with the wavelength of the incident light.

Once the heat is generated by metallic nanostructures upon laser irradiation, a heat flux is created within the surrounding medium and the resultant temperature field is given by [34, 35]

$$\rho C_P \frac{\partial T(\boldsymbol{r})}{\partial t} - \nabla \cdot [\tau \nabla T(\boldsymbol{r})] = q \qquad (1)$$
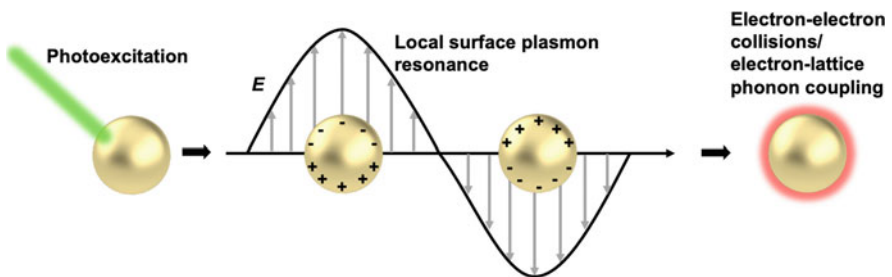

Fig. 1 Schematic of plasmonic photothermal effects. When laser irradiates metallic nanoparticles with suitable wavelengths, localized surface plasmon resonance is activated and the collective oscillation of electrons increases the frequency of collisions for the formation of local heating

where ρ, C_P and τ are the density, specific heat capacity at constant pressure and thermal conductivities of the corresponding regions, respectively. q is the heat power density of the plasmonic nanostructure. Since the metallic nanostructures possess high thermal conductivity while the environmental medium, typically aqueous solutions, has a low thermal conductivity, the temperature field within a single nanostructure will be uniform while a temperature gradient field is attained in the vicinity of the nanostructure. The continuous laser irradiation leads to a steady temperature distribution, which is established at nanosecond timescales. At the steady state, Eq. (1) can be written as $\nabla \cdot [\tau \nabla T(\boldsymbol{r})] = -q$. Besides, Q and q can be associated according to Poynting's theorem [36]:

$$Q = \iiint q \mathrm{d}V \tag{2}$$

where $q = \frac{1}{2} \mathrm{Re} \left(\boldsymbol{J} \cdot \boldsymbol{E}^* \right), \boldsymbol{J} = \sigma \boldsymbol{E}$ and $\boldsymbol{E}$ represent the electronic current density and electric field inside the metallic nanostructure, respectively; σ is the conductivity of the structure. Accordingly, numerical simulations can be performed to explore the C_{abs} and the temperature distribution based on the material properties of certain nanostructures [37].

As for trapping and tweezing of particles via plasmonic photothermal effects, plasmonic substrates composed of nano-sized metallic components are usually exploited for efficient heat generation and retention [38–40]. One popular type of plasmonic substrates called gold nano-islands (AuNIs) is shown in Fig. 2a, which consist of quasi-continuous Au nanoparticles fabricated by annealing Au thin films [38, 41]. Compared with Au thin films, AuNIs can create stronger temperature gradient fields upon laser irradiation due to the localized plasmonic resoances and the low thermal conductivity among each isolated Au nanoparticles (Fig. 2b) [38, 42]. The surface plasmon resonance wavelength of certain AuNIs can be tuned through adjusting the annealing temperature, rate of annealing, and thickness of original Au films.

More precise heat management of plasmonic substrates can be achieved by rationally designing the shape and spatial distribution of metallic nanoparticles. For instance, Au nanorods (AuNRs) on glass substrates have been successfully fabricated and exploited for heat-mediated particle manipulation (Fig. 2c) [39]. When the laser beam irradiates on certain AuNRs, a high-resolution temperature gradient field is established around the AuNRs (Fig. 2d). Similar to AuNIs, the surface plasmon resonance wavelength can be changed by the aspect ratio and size of AuNRs. In addition, the temperature gradient field of AuNRs can be further tuned by the polarization of incident light because the activated resonance modes, e.g., transversal and longitudinal resonances, is relevant to the relative angle between the electric field vector of incident light and the long axis of rods (Fig. 2e). Moreover, local plasmonic heating can also be achieved by metallic nanohole arrays [27, 40, 43]. Due to the in-plane Bloch mode surface plasmon polaritons [44, 45] and localized surface plasmon resonance of the individual nanoholes, the excitation of electric fields and resultant temperature gradient fields are usually concentrated
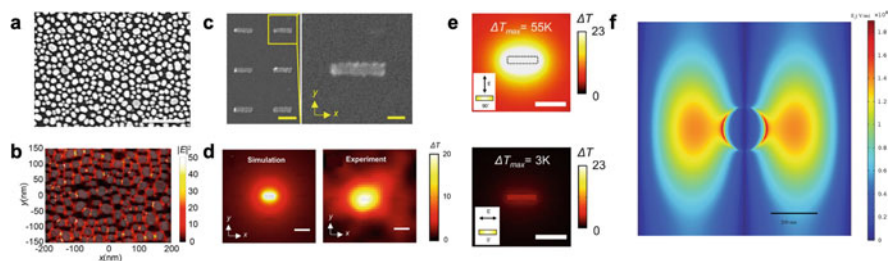
Fig. 2 Three representative metallic nanostructures for plasmon-enhanced optothermal manipulation. (**a**) Scanning electron microscopy (SEM) image of gold nano-islands. Scale bar: 200 nm. Adapted with permission from Ref. [28]. Copyright 2018 Springer Nature. (**b**) Simulated electric field distribution of AuNIs upon laser irradiation by finite-difference time-domain (FDTD) simulations. The model for the substrate was imported from the SEM image of AuNIs. Adapted with permission from Ref. [46]. Copyright 2017 American Chemical Society. (**c**) SEM images and (**d**) temperature field distribution of gold nanorods. (**e**) Simulated temperature field distribution with the electric field of incident light perpendicular (top) and parallel (bottom) to the long axis of the nanorod. The temperature fields were obtained from the FDTD-simulated electromagnetic fields. Scale bar: (**c**) left 300 nm, (**c**) right 100 nm, (**d**) 1 μm and (**e**) 500 nm. Adapted with permission from Ref. [39]. Copyright 2018 American Chemical Society. (**f**) Electric field distribution of nanohole arrays. The simulated temperature fields were modelled by finite element method (COMSOL Multiphysics). Scale bar: 200 nm. (Adapted with permission from Ref. [40]. Copyright 2018 American Chemical Society)

near the rims and interspace of nanoholes (Fig. 2f). In addition to nanorods and nanoholes, many other metallic nanostructures (such as nanobowties) have been designed and fabricated [34] for subtle control of local plasmonic heating.

3   Opto-Thermophoretic Manipulation

Opto-thermophoretic manipulation relies on the thermophoretic motion of targeted objects under optically generated temperature gradient fields. Depending on the thermophobicity and thermophilicity of targeted objects, different plasmonic nanostructures have been designed to create highly localized temperature gradient fields with either hot or cold center to trap molecules and colloidal particles.

3.1   Mechanism

Thermophoresis, also known as the Soret effect, describes the directed migration of suspended colloidal particles or micelles along a temperature gradient (Fig. 3) [47–49]. The drift velocity of colloidal particles is given by

Fig. 3 Schematic of thermophoresis. Suspended particles or molecules with different signs of the Soret coefficient S_T show directed migration toward cold/hot regions
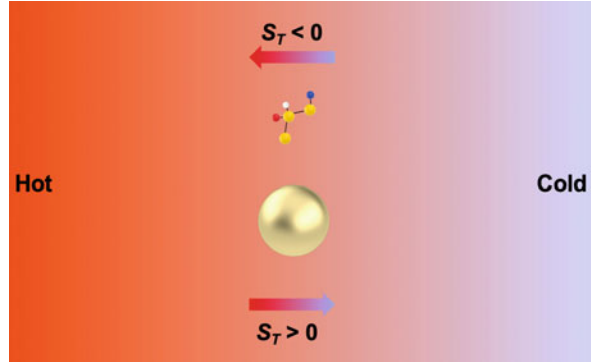
$$\boldsymbol{u} = -D_T \nabla T \tag{3}$$

where D_T is the thermophoretic mobility and ∇T is the temperature gradient. As for dilute suspensions in a steady state, the concentration gradient ∇c is expressed as [48]

$$\nabla c = -c \frac{D_T}{D} \nabla T = -c S_T \nabla T \tag{4}$$

where c is the concentration of the suspended particles, D is the Brownian diffusion coefficient, and S_T is the Soret coefficient. Since D of different components in a solution varies significantly, the Soret coefficient S_T is commonly utilized for the description of thermophoresis. Specifically, $S_T > 0$ describes that suspended objects are thermophobic and migrate toward the cold regions along the temperature gradient while $S_T < 0$ implies that suspended objects are thermophilic, which move to the hot region under ∇T.

3.2   Techniques and Applications

Most colloidal particles and molecules are thermophobic [50–52], moving from the hot to the cold regions. In order to stably trap suspended objects with $S_T > 0$ via thermophoretic migration, a localized "temperature well" should be created with the center being cold [29, 53, 54], which can be established when a non-absorbing region is surrounded by plasmonic nanostructures while a focused laser beam illuminates on the rim of the nanostructure selectively. Accordingly, Braun et al. have demonstrated opto-thermophoretic trapping of single DNA molecules within a hole surrounded by gold thin films based on feedback-controlled laser illumination (Fig. 4a) [29]. The effective potential energy $U_{eff}\left(\overrightarrow{r}\right)$ of thermophoretic trapping is given by [29]

$$U_{eff}\left(\overrightarrow{r}\right) = k_B T_0 S_T \Delta T\left(\overrightarrow{r}\right) \tag{5}$$

where k_B is Boltzmann constant, T_0 is ambient temperature, and $\Delta T\left(\overrightarrow{r}\right)$ is the local temperature increment. Since the effective potential is mainly determined by the temperature profile, a feedback control rule about steering the focused laser beam has been adopted to increase the temperature gradient within the metallic hole structure (Fig. 4b), which improves the trapping stiffness by a factor of 12. Specifically, compared with simply heating the whole rim of the Au nanostructure, the optically heating spot is dynamically controlled based on an acousto-optic deflector by analyzing the real-time position of the targeted object, whose width of the Gaussian position distribution can decrease by a factor of 3.5, and unwanted temperature rises at the trapping center can be alleviated. Moreover, different trapping modes, i.e., off-center trapping, two-position trapping, circular line trapping, and trapping at an expanded area, were also achieved based on different feedback laser manipulation protocols (Fig. 4c). Recently, Cichos and co-workers exploited similar methods to thermophoretically trap single amyloid fibril for the observation of fibril growth, secondary nucleation and/or fibril breakup [54].

The above opto-thermophoretic trapping enables the manipulation of single and multiple thermophobic macromolecules or colloids by elaborating the plasmon-enhanced temperature gradient field. However, targeted objects can only be trapped inside a plasmonic nanostructure, lacking dynamic manipulation over large areas. Opto-thermophoretic tweezers can be achieved if suspended objects become thermophilic, i.e., the objects can be attracted toward and stably trapped at the plasmonic heating region. Recently, Lin et al. have demonstrated opto-thermophoretic tweezers by exploiting the entropic responses and permittivity gradients at the particle-solvent interface under a plasmon-enhanced thermal gradient field [55]. Since the Brownian diffusion coefficient D is always positive, the key to opto-thermophoretic tweezers is to make targeted particles have negative D_T. The thermophoretic mobility is given by [56]

$$D_\mathrm{T} = -\frac{\varepsilon}{2\eta T}\frac{2\Lambda_1}{2\Lambda_1 + \Lambda_\mathrm{P}}\left(1 + \frac{\partial ln\varepsilon}{\partial lnT}\right)\zeta^2 \tag{6}$$

where ε is the solvent permittivity, η is the solvent viscosity, T is the temperature, Λ_1 and Λ_P is the thermal conductivities of the solvent and the particle, and ζ is the zeta potential of the particle, respectively. In bulk water, $\tau = \frac{\partial ln\varepsilon}{\partial lnT}$ is equal to -1.4 at room temperature, which indicates that the suspended particles are thermophobic. However, for charged particles, polarized water molecules can be confined in the electric double layer and enable abnormal permittivity, which is smaller than that of bulk water and leads to a positive τ value (Fig. 5a). Therefore, suspended charged particles have a negative D_T, which will be attracted and trapped at the heating spot. By exploiting Au nanodisk arrays as the heating substrate, plasmonic hotspots can be created selectively over large areas, and charged polystyrene beads can be dynamically transported (Fig. 5b). It is worth noting that plasmon-enhanced optical
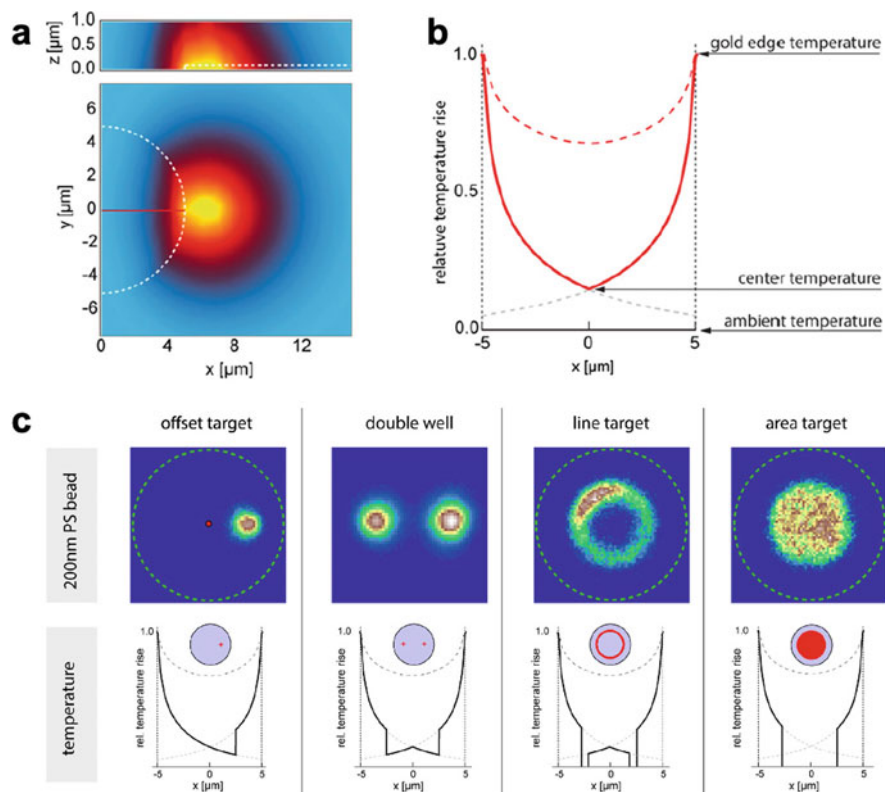
Fig. 4 Opto-thermophoretic trapping of objects with $S_T > 0$**.** (**a**) Simulated temperature profile with a focused laser beam illuminating at the rim of a gold structure. The white dash line indicates the boundary between the gold thin film and the glass. (**b**) Calculated relative temperature rise profile. The red dash line corresponds to the steady-state profile when the whole gold structure is heated. The solid line depicts the scaled temperature rise profile when the focused laser beam is controlled by a feedback program. The grey dash line extends the solid red line to indicate the profile without position feedback, i.e., only one spot is heated. (**c**) Different thermophoretic trapping potentials generated by different feedback rules. The simulated temperature fields were modelled by finite element method (COMSOL Multiphysics). (Adapted with permission from Ref. [29]. Copyright 2015 American Chemical Society)

force is excluded here since the calculated optical force is only 4 fN for a 500 nm PS particle with the same laser power, which is insufficient to trap the particle. Opto-thermophoretic tweezers are also applicable to biological objects due to the existence of phospholipid bilayers and the resultant negative surface charge (Fig. 5c) [46, 57]. Parallel manipulation of yeast cells has been achieved by exploiting a digital micromirror device (DMD) (Fig. 5d). Recently, Peng et al. studied opto-thermophoretic trapping of colloidal particles in different non-ionic liquids and reveal that the driving forces of opto-thermophoretic tweezers stem from a layered structure of solvent molecules at the particle-solvent interface. The trapping stability
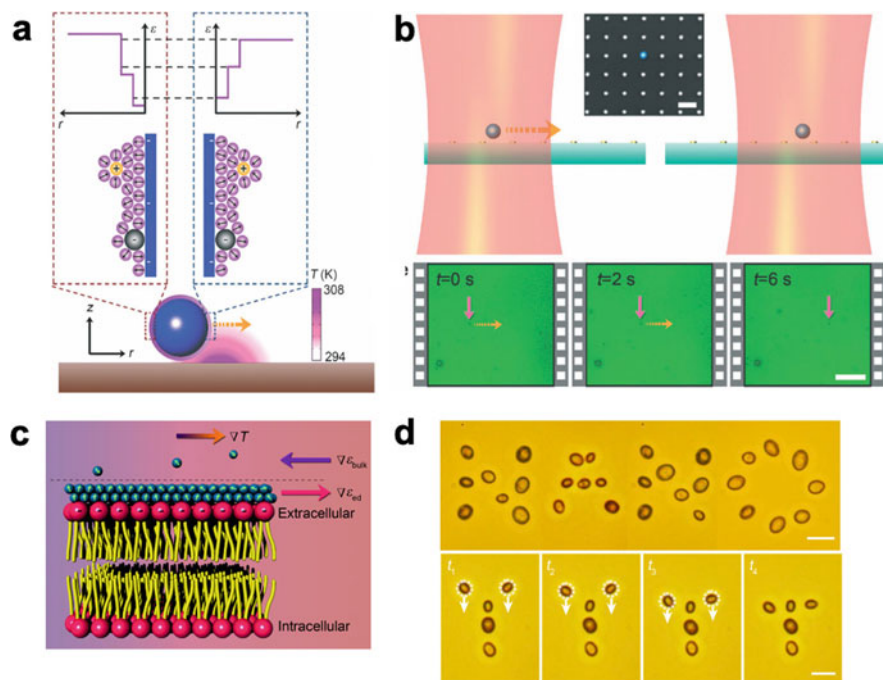
Fig. 5 Opto-thermophoretic trapping of objects with $S_T < 0$. (a) Schematic of the working principle of entropy-driven opto-thermophoretic tweezers. The purple balls correspond to the water molecules with their dipole orientations. The charged balls indicate anions and cations, respectively. **(b)** Schematic and optical images show light-directed thermophoretic transport of a single 500 nm polystyrene (PS) bead over Au nanodisk arrays. Scale bar: 10 μm. (Adapted with permission from Ref. [55]. Copyright 2017 The Royal Society of Chemistry). **(c)** Schematic shows the change of the permittivity in the electric double layer on a cell membrane under a temperature gradient field. **(d)** Parallel thermophoretic manipulation of yeast cells in "NANO" patterns (top) and "Y" to "T" transformation (bottom). Scale bar: 10 μm. (Adapted with permission from Ref. [46]. Copyright 2017 American Chemical Society)

of particles can be enhanced by designing the particle hydrophilicity, particle surface charge, solvent type, and ionic strength on the layered interfacial structures [58].

4 Opto-Thermoelectric Manipulation

Plasmon-enhanced thermophoresis can not only be directly exploited for particle manipulation but also enables the controlled migration of cations and anions, leading to the formation of thermoelectric fields in solutions. By engineering the plasmonic nanostructures and electrolyte composition, the opto-thermo-electro-mechanical coupling can be utilized to achieve opto-thermoelectric trapping and tweezing with low operational optical power, simple optical setup, and applicability to a wide range of polymers, metals, semiconductors, and dielectric nanostructures

Fig. 6 Schematic of liquid thermoelectricity. Cations (red circles with "+" symbols) and anions (blue circles with "−" symbols) have thermophoretic motions under a temperature gradient. The resultant thermoelectric field $\boldsymbol{E}$ induces directed migration of suspended charged particles (golden spheres with "+" symbols)
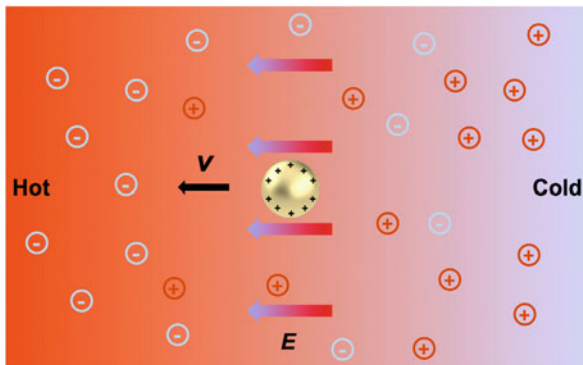
with different sizes and shapes. Compared to the conventional one-dimensional heating approach [20], exploiting plasmonic nanostructures can lead to radially shaped opto-thermoelectric fields, enabling particle manipulation at single-particle resolution.

4.1 Mechanism

When a localized temperature gradient field is formed in a solution, cations and anions drift towards either the hot or the cold region with different velocities based on their different S_T Eq. (4). As the ionic redistribution reaches a steady state, an electric field is built along the temperature gradient, driving suspended charged particles drifting directionally (Fig. 6). The underlying principle of the particle migration in aqueous environments is termed liquid thermoelectricity or the electrolyte Seebeck effect. Generally, the thermoelectric field can be given by [59, 60]

$$\boldsymbol{E}_{\text{TE}} = \frac{k_B T \nabla T}{e} \frac{\sum_i Z_i n_i S_{Ti}}{\sum_i Z_i^2 n_i} \qquad (7)$$

where i indicates the ionic species, k_B is the Boltzmann constant, T is the environmental temperature, e is the elemental charge, and Z_i (± 1 for positive and negative monovalent ions), n_i, as well as S_{Ti} represent the charge number, the concentration, and the Soret coefficient of i species, respectively. Moreover, the thermophoretic mobility D_T of charged particles under the thermoelectric field is obtained via [59, 61]

$$D_T = \frac{\varepsilon \zeta^2}{3\eta T} - \frac{\varepsilon \zeta}{\eta} S \qquad (8)$$

where ε and η are the permittivity and viscosity of the solution respectively, ζ is the surface potential of the particle, and S is the Seebeck coefficient that can be expressed as $S = E_{\mathrm{TE}}/\nabla T$. It should be noted that the first term is always positive, which is related to the thermo-osmotic flow [62, 63]; while the second term can either be positive or negative, depending on the thermoelectric field and the surface charge of suspended particles. Therefore, according to Eq. (3), charged objects can move toward the hot/cold regions due to the liquid thermoelectricity, which can be tuned as a function of the electrolyte composition [64], ionic strength [49], temperature [65, 66], particle-solvent interface [50], colloidal size [67], and particle concentration [68, 69].

4.2 Techniques and Applications

Opto-thermoelectric effect has been proposed to achieve directional transportation of colloidal particles [64], micelles [70], DNA [60], and so forth [56, 71, 72]. Localized plasmonic heating is usually exploited to build inward/outward thermo-electric fields in the vicinity of the illuminated plasmonic nanostructures. Since the direction of the thermoelectric field is mainly determined by the electrolyte solution, opto-thermoelectric trapping is limited to either positively or negatively charged particles. Recently, Lin et al. overcame this challenge and developed opto-thermoelectric tweezers by exploiting cetyltrimethylammonium chloride (CTAC) solutions to manipulate various colloidal particles with different sizes, shapes and materials regardless of their original surface charge properties [28]. When colloidal particles are suspended in CTAC solutions, the CTA^+ molecules can not only self-assemble into positive micellar ions but also modify all particles with positive surface charges (Fig. 7a). As the laser beam illuminates on the plasmonic nanostructures (AuNIs), the difference in the Soret coefficients of positive micellar ions and negative Cl^- ions (S_T (micelle) $\gg S_T$ (Cl^-)) leads to the spatial charge separation and a resultant thermoelectric field pointing toward the laser beam (Fig. 7b). Therefore, positively charged colloidal particles are attracted and stably trapped at the laser-illuminated region [73, 74]. Since AuNIs is quasi-continuous, opto-thermoelectric manipulation of colloidal particles is achieved by moving the heating laser or the sample stage. Parallel manipulation of metallic nanoparticles was further realized with a DMD that can generate multiple laser beams, i.e., simultaneously creating several plasmonic heating spots (Fig. 7c). When the AuNIs are implanted to the tapered optical fiber, the nanoparticles can be trapped at the fiber tip and transported to targeted objects in a 3D manner (Fig. 7d) [75].

To overcome the optical diffraction limit for higher spatial resolution of opto-thermoelectric manipulation, Liu et al. applied Au nanoantennas to trap nanopar-ticles at subwavelength resolution [39]. Since the thermoplasmonic response of nanoantennas depends on the polarization of incident laser beam relative to the long axis of nanoantennas, the intensity of thermoelectric fields and resultant trapping stiffness can be tuned by the polarization of the laser beam. Accordingly,
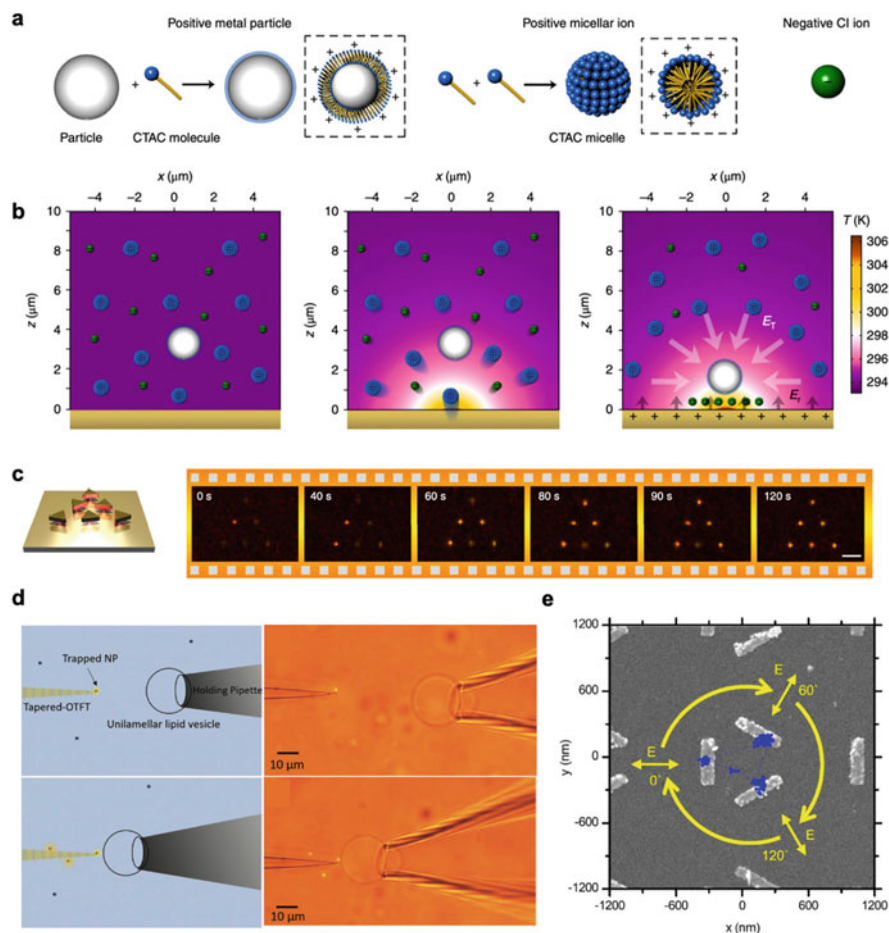
Fig. 7 Opto-thermoelectric trapping and manipulation. (**a**) Schematic shows the surface modification process of suspended particles by CTAC molecules and the formation of positively charged CTAC micelles through self-assembly. (**b**) Schematic demonstrates the formation of localized thermoelectric fields in the vicinity of a laser-induced plasmonic hotspot. (**c**) Schematic and dark-field optical images show an array made of anisotropic Au nanotriangles. Scale bar: 5 μm. (Adapted with permission from Ref. [28]. Copyright 2018 Springer Nature). (**d**) Schematics and optical images demonstrate three-dimensional nanoparticle delivery through fiber-based opto-thermoelectric trapping. (Adapted with permission from Ref. [75]. Copyright 2019 De Gruyter). (**e**) Opto-thermoelectric manipulation of nanoparticles based on plasmonic nanoantennas. Particles are circularly transported among different nanoantennas by changing the light polarization. (Adapted with permission from Ref. [39]. Copyright 2018 American Chemical Society)

circular transportation among three Au nanoantennas was achieved by altering the polarization angle of the laser beam (Fig. 7e).

Moreover, the CTAC molecules can serve as depletants to induce depletion forces for opto-thermoelectric assembly [76–80]. Specifically, when multiple particles

are trapped at the hotspot closely, CTAC micelles escape from interparticle gaps, creating concentration gradients and exerting an osmotic pressure on the particles to bond the particles. Different nanostructures, including chiral metamolecules [76] and 3D colloidal structures [78], are precisely fabricated in a bottom-up fashion and can be further immobilized by photocurable hydrogels [79]. More details can be found in other relevant reviews [30, 81–84].

5 Thermo-plasmonic Convection-Assisted Manipulation

Plasmonic tweezers have been developed for over a decade as an evolutionary optical manipulation technique because of their sub-diffraction-limited resolution [10–12]. However, since the near-field optical gradient force only takes effect within a nanoscale working distance, it is challenging for plasmonic tweezers to effectively trap suspended particles in solution with low particle concentrations (e.g. 2×10^7 particles·ml^{-1}). Recently, thermo-plasmonic convection generated by plasmonic nanostructures has been exploited to achieve fast transport of particles towards plasmonic hotspots, which significantly improves the trapping efficiency of plasmonic trapping.

5.1 Mechanism

Thermo-plasmonic convection describes a type of natural convection induced by local heated fluid. Specifically, when a thermal gradient is built around a plasmonic nanostructure via laser irradiation, the fluid density surrounding the heated structure decreases as the fluid temperature increases, leading to upward motion because of buoyancy. Subsequently, owing to the fluidic continuity, the fluid neighboring the local heated fluid flows towards the hotspot, being heated and moving upwardly again. Thus, a convective flow is generated in the vicinity of the laser-illuminated plasmonic nanostructure (Fig. 8a and 8b), which can be exploited for rapid particle delivery.

Donner et al. conducted a comprehensive study to analyze the plasmon-enhanced natural convection theoretically and numerically [85]. It has been validated that for thermoplasmonics occurring at the macro- or nano-scale in water-like media (i.e., the fluidic flow possessing small Reynolds number and Rayleigh number), the temperature distribution of fluid in the vicinity of heated nanostructures can be simplified as [85]

$$\partial_t T\left(\mathbf{r}, t\right) - \alpha \nabla^2 T\left(\mathbf{r}, t\right) = 0 \tag{9}$$

where $T(\mathbf{r}, t)$ represents the temperature distribution of the fluid, and α is the fluid diffusivity. Meanwhile, the Navier-Stoke equation describing the fluid velocity [86] is further reduced to [85]
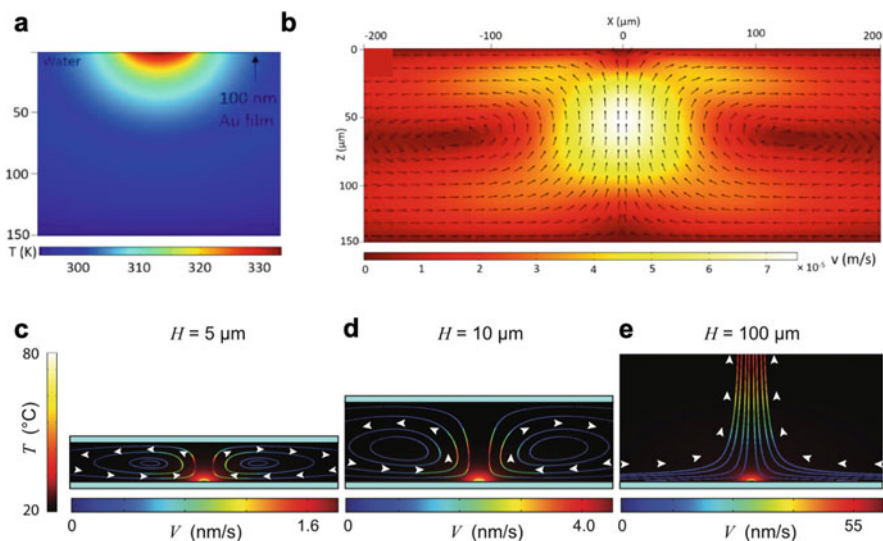
Fig. 8 Formation of thermo-plasmonic convection based on microscale plasmonic heating.
(**a**) Simulated temperature distribution around a single nanoaperture on a 100 nm Au film that
is irradiated over a circular area with diameter ∼ 60 μm and (**b**) corresponding simulated
convective flow velocity distribution. The temperature field was obtained from the FDTD-
simulated electromagnetic field, and the fluid velocity map was achieved by computational fluid
dynamics (CFD) simulations. (Adapted with permission from Ref. [27]. Copyright 2019 American
Chemical Society). (**c**)–(**e**) Simulated velocity distribution with various chamber heights H. The
plasmonic nanostructure is a gold disk of radius r = 250 nm and T = 80 °C. The velocity field
was obtained by using finite element method (COMSOL Multiphysics). (Adapted with permission
from Ref. [85]. Copyright 2011 American Chemical Society)

$$\partial_t \mathbf{v}\left(\mathbf{r}, t\right) - \nu \nabla^2 \mathbf{v}\left(\mathbf{r}, t\right) = \mathbf{f}_t\left(T\left(\mathbf{r}, t\right)\right) \tag{10}$$

where $\mathbf{v}(\mathbf{r}, t)$ is the fluid velocity, ν is the fluid viscosity and $\mathbf{f}_t(T(\mathbf{r}, t))$ represents
the force per unit mass due to temperature gradient that is commonly given as
$\mathbf{f}_t(T) = \beta g(T(\mathbf{r}, t) - T_\infty)\mathbf{u}_z$ with g being the gravitational acceleration, β being
the dilatation coefficient of water and $\mathbf{u}_z$ demonstrating the unit vector along the
z-direction.

It's worth noting that the fluid velocity generated by single plasmonic nanos-
tructures with a typical size below 200 nm is estimated to be less than 10 nm/s
even if the fluid temperature is close to the boiling point, which can hardly be
exploited for effective particle delivery owing to the existence of Brownian motions
or thermophoresis. Thus, thermo-plasmonic convection-assisted trapping usually
requires micro-sized plasmonic nanostructures to be illuminated. Moreover, the
shape and velocity of fluid can also be tuned by the height of the chamber (Fig.
8c-8e).

5.2   Techniques and Applications

Since thermo-plasmonic convection induced by plasmon-enhanced thermal effect often works under large-area illumination, it can be utilized for quick delivery and local concentration of targeted objects in solution over large volumes, especially for ultra-low concentration conditions. Recently, Kotnala et al. adopted thermo-plasmonic convection to facilitate plasmonic trapping and sensing of particles within an ultralow concentration ($< 2 \times 10^7$ particles·ml^{-1}) [27]. As shown in Fig. 9a, a multimode optical fiber coupled with a 532 nm laser beam illuminates a Au nanoaperture to generate the thermo-plasmonic convection with high velocity (~10–20 µm·s^{-1}). Dispersed particles were transported toward the plasmonic nanoaperture via the convective flow and got trapped with a 1020 nm laser beam (Fig. 9b). Compared with diffusion-limited plasmonic trapping, thermo-plasmonic convection-assisted trapping can reduce the trapping time by five-fold and 15-fold for particle concentrations of 2×10^8 and 2×10^7 particles·ml^{-1}, respectively (Fig. 9c). The particle delivery time can further be decreased by increasing the flow velocity. However, the convective velocity should be determined by the trapping laser intensity so that the drag force does not dominate over the near-field optical gradient force, which leads to the failure of single-particle trapping at the nanoaperture (Fig. 9d).

As the convective flow can have a vertical velocity component perpendicular to the substrate, it can also be utilized to assist 3D optical manipulation of colloidal particles and biological objects [87–89]. Cong et al. exploited a gold-coated micro-well array for efficient optical trapping and single-cell analysis [89]. In this work, the laser heating not only triggers thermo-plasmonic convective flow to facilitate the upward movement of a single living cancer cell, but also offers a constant temperature environment for recombinase polymerase amplification reaction of nucleic acid markers. In addition, thermo-plasmonic convective flow can also be generated by mobile plasmonic nanoparticles dispersed in solution, which assists the concentration and patterning of nanoparticles for photothermal convection lithography on generic substrates [90].

6   Marangoni Convection-Assisted Manipulation

In addition to thermo-plasmonic convection, Marangoni convection is another approach to facilitating long-range particle delivery for effective plasmonic trapping of nano-objects. Different from thermo-plasmonic convection induced by density gradient of a heated solution, Marangoni convection relies on the gradient of surface tension at the interface between two fluids, which usually have higher flow velocity. Moreover, the Marangoni convection induced by plasmonic heating can also be directly used for particle trapping and manipulation.
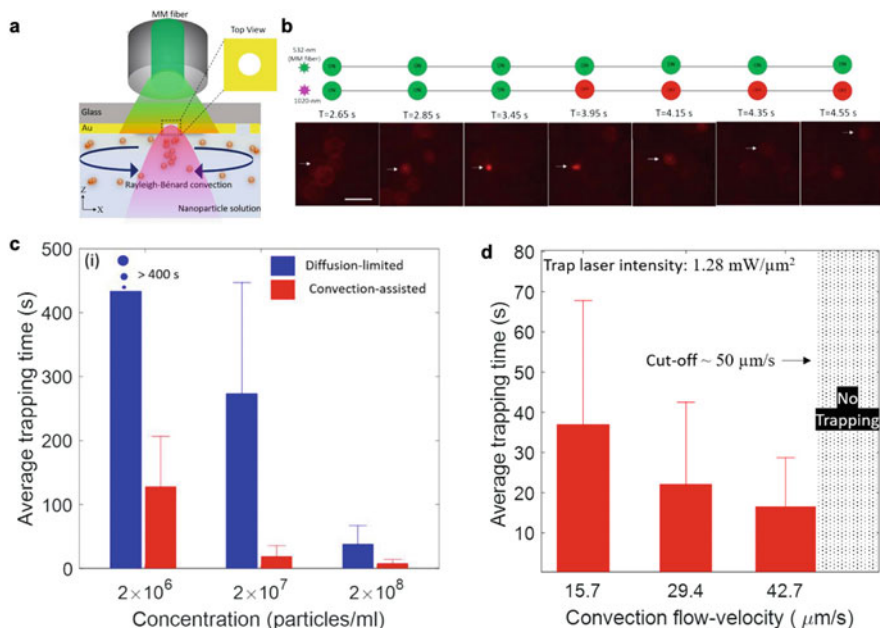
Fig. 9 Thermo-plasmonic convection-assisted trapping and tweezing. (**a**) Schematic shows that a multimode fiber illuminates a large area of AuNIs with nanoapertures for the formation of thermo-plasmonic convection. (**b**) Dark-field images demonstrates thermo-plasmonic convection-assisted trapping and release of a single 200-nm fluorescent polystyrene nanoparticle within a circular nanoaperture surrounding by AuNIs. 532-nm laser is used to generate the convective flow while 1020-nm laser is for the plasmonic optical trapping. Scale bar is 25 μm. (**c**) Comparison of average trapping time of diffusion-limited and convection-assisted trapping at three different particle concentrations. (**d**) Diagram represents the impact of convection-flow velocity on the average particle-trapping time. (Adapted with permission from Ref. [27]. Copyright 2019 American Chemical Society)

6.1 Mechanism

Marangoni convection describes mass transfer along with an interface between two fluids due to a gradient of the surface tension, which can be attributed to the concentration gradient or temperature gradient, where the latter type is also termed as thermocapillary convection [91]. In brief, when a laser beam irradiates the plasmonic nanostructures with a relatively high power intensity, abundant heat is generated at the hotspot, leading to water evaporation and resultant vapor bubble nucleation at the liquid-substate interface [92, 93]. As the surface tension is inversely related to the temperature, a gradient of surface tension exists at the liquid-vapor interface due to the temperature gradient (Fig. 10a). Thus, a convective flow is generated around the microbubble because of the fluid's continuity (Fig. 10b). The temperature distribution and flow velocity pattern are different if the relative size between the diameter of the bubble and the chamber thickness changes (Fig.
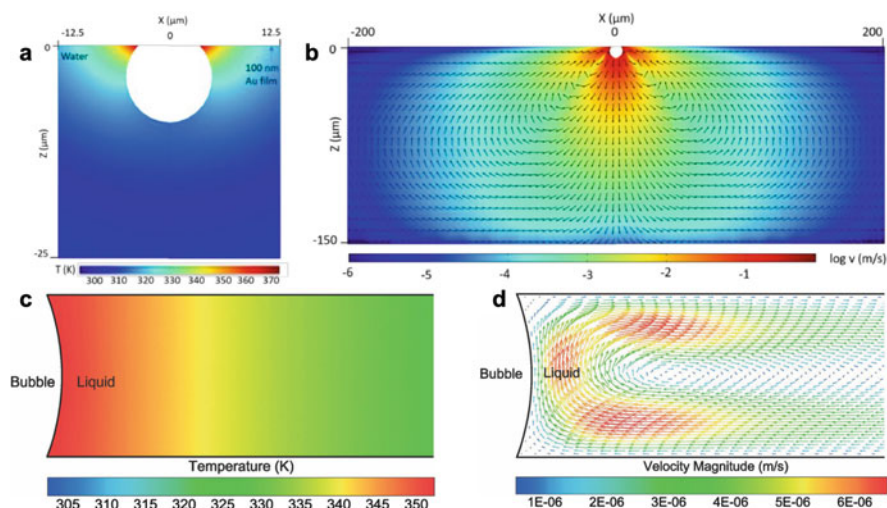
Fig. 10 Formation of Marangoni convection based on plasmonic heating. (**a**) Simulated temperature distribution and (**b**) simulated flow velocity around a 10 µm bubble generated upon laser irradiation on AuNIs. The temperature field was obtained from the FDTD-simulated electromagnetic field, and the fluid velocity map was achieved by CFD simulations. (Adapted with permission from Ref. [27]. Copyright 2019 American Chemical Society). (**c**) Simulated temperature distribution and (**d**) simulated flow velocity of a 60 µm vapor bubble generated in a chamber with height being 70 µm. The temperature distribution and fluid velocity map were achieved by CFD simulations (ANSYS Fluent). (Adapted with permission from Ref. [95]. Copyright 2014 Royal Society of Chemistry)

10c, d). Besides, it's worth noting that the plasmonic heating-induced Marangoni convection can also occur at the planar air-liquid interface via floating plasmonic nanoparticles [94].

6.2 Techniques and Applications

Similar to thermo-plasmonic convection, Marangoni convection has also been exploited for rapid delivery of nanoparticles toward the plasmonic hotspot for efficient plasmonic trapping (Fig. 11a). Kotnala et al. employed two laser beams to actuate Marangoni convection and plasmonic trapping, respectively, which significantly enhanced the trapping efficiency of conventional nanoaperture-based plasmonic tweezers [27]. Specifically, a 532 nm laser is used for plasmonic heating and bubble generation, while a 1020 nm laser works for plasmonic trapping. It's worth noting that the 532 nm laser beam should be turned off after the bubble emerges for 1–2 s in case that the nanoparticles are directly printed on the substrate by the strong Marangoni convective flow [96]. Due to the long-range delivery of nanoparticles via Marangoni convection, the average particle-trapping time can
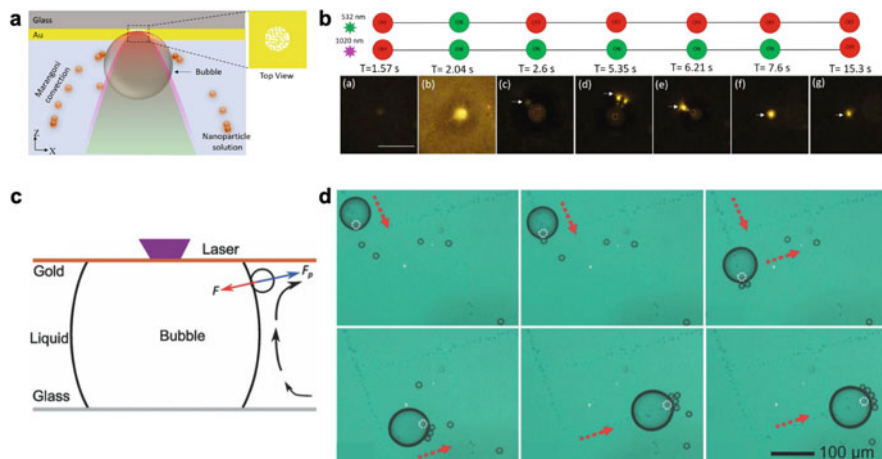
Fig. 11 Marangoni convection-assisted trapping and tweezing. (**a**) Schematic shows suspended nanoparticles being delivered to the nanoaperture via bubble-based Marangoni convection and get trapped by plasmonic tweezers. (**b**) Time-evolved dark-field images demonstrates bubble-assisted trapping and release of a single 200 nm fluorescent PS nanoparticle. 532 nm laser is exploited for the bubble generation while 1020 nm laser is specifically for plasmonic trapping. Scale bar: 10 μm. (Adapted with permission from Ref. [27]. Copyright 2019 American Chemical Society). (**c**) Schematic shows that particle get stabilized on the bubble surface via the balance between the pressure force (F_P) and the surface tension force (F). (**d**) Time-lapse optical images show the particle collection process via the movement of the bubble. (Adapted with permission from Ref. [95]. Copyright 2014 The Royal Society of Chemistry)

be reduced by 40 ~ 80 folds compared with that of diffusion-limited trapping. Moreover, since the position of the gas bubble can follow the movement of the heating laser on continuous plasmonic nanostructures [97], suspended particles can be patterned on the plasmonic substrate continuously for nanoparticle writing, namely bubble printing [98–102].

In addition to particle concentration, Marangoni convective flow can also facilitate precise trapping and manipulation of colloidal particles and biological cells [95, 103–105]. Zhao et al. developed single-particle trapping and manipulation based on the optothermal bubble [95]. When the bubble is generated upon laser irradiation on a gold thin film, neighboring suspended particles are attracted towards the bubble due to the Marangoni convection. Once the particle is attached to the bubble surface, it will be trapped stably through the balance among the surface tension force, pressure force and drag force (Fig. 11c). Particle collection and transportation were further demonstrated via directly manipulating the bubbles as a shuttle (Fig. 11d).

7 Electrothermoplasmonic Flow-Assisted Manipulation

When a laser beam irradiates a plasmonic nanostructure, in addition to thermophoresis and natural convection take effect, a gradient of permittivity and electrical conductivity can also be obtained in the vicinity of the nanostructure due to the local temperature gradient. Once an additional a.c. electric field is applied, electric body force is triggered and the force can be given by $f = \rho_f \boldsymbol{E}_l - \frac{1}{2}|\boldsymbol{E}_l|^2 \nabla \varepsilon_m$ for an electrically linear incompressible fluid [106, 107], where ρ_f is the volume density of induced free charges, $\boldsymbol{E}_l$ represents the local electric field, while $\nabla \varepsilon_m$ is the gradient of the fluid's permittivity. The electric body force can trigger a new type of fluidic flow termed as ETP flow, which can also be exploited for trapping and tweezing of objects at single-particle resolution.

7.1 Mechanism

ETP flow describes a new type of opto-microfluidic flow for particle and molecule manipulation, which mainly stems from the electric body force in the fluids with assistance from plasmon-enhanced thermal effects [33, 40, 43]. Specifically, when a laser beam irradiates on plasmonic nanostructures, the plasmonic heating creates a local gradient of fluid's permittivity and electrical conductivity. Through applying an external a.c. electric field, an electrical body force per unit volume in the locally heated fluid is significantly enhanced. The resultant motion of the fluid will then exert a drag force on suspended particles, which can transport suspended particles toward the plasmonic hotspot (Fig. 12a). Although the plasmonic optothermal effect can intrinsically lead to buoyancy force for the generation of thermo-plasmonic convection [108], the electric body force plays an essential role in the ETP flow, which is given as [33]

$$\langle F_{\text{ETH}} \rangle = \frac{1}{2}\epsilon \left[\frac{(\alpha - \gamma)}{1 + (\omega\tau)^2} \left(\nabla T \cdot \boldsymbol{E} \right) \boldsymbol{E} - \frac{1}{2}\alpha |\boldsymbol{E}|^2 \nabla T \right] \tag{11}$$

where $\alpha = (1/\epsilon)(\partial\epsilon/\partial T)$, $\gamma = (1/\sigma)(\partial\sigma/\partial T)$, $\tau = \epsilon/\sigma$, ϵ and σ are the fluid's permittivity and electrical conductivity, respectively, and ω is the frequency of the a.c. electric field. Accordingly, the ETP flow can not only be tuned by the plasmonic heating but also the frequency and amplitude of the a.c. electric field. Numerical simulations further confirm that the ETP flow scales linearly with applied laser power but scales quadratically with the a.c. electric field. The fluid radial velocity of the ETP flow is validated to be two orders of magnitude larger than that of thermo-plasmonic convection, implying that the ETP flow is dominant here for on-demand long-range and rapid delivery of single nano-objects.
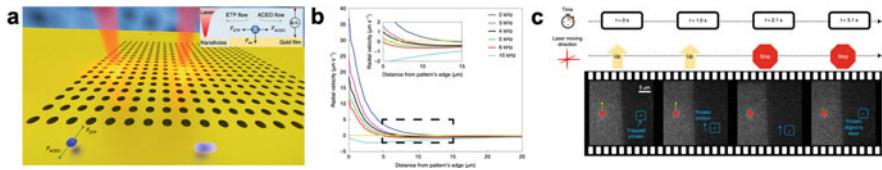
Fig. 12 Demonstration of electrothermoplasmonic flow-assisted trapping and tweezers. (**a**) Schematic shows the working mechanism of opto-thermo-electrohydrodynamic tweezers. (**b**) Simulated radial velocity under different a.c. frequencies along the direction perpendicular to the length of the nanohole array. The inset shows the zoom-in black dash box. The position of the stagnation zone can be tuned by the a.c. frequency. (**c**) Optical images show the dynamic manipulation of a single bovine serum albumin (BSA) protein molecule. (Adapted with permission from Ref. [43]. Copyright 2020 Springer Nature)

7.2 Techniques and Applications

ETP flow can transport suspended nano-objects towards the plasmonic nanoantenna at the fluid's velocity $\sim$ 10–15 μm s^{-1} [33], which can then be trapped at the nanostructure surface via the optical gradient force [11]. Once the targeted object is trapped at the surface, there have three options for subsequent manipulation: (1) laser on but electric field off: maintain the object being trapped via optical gradient force with minimum energy consumption; (2) both laser and electric field off: release the object; (3) laser on but switch a.c. field to d.c. field temporarily: immobilize the object on the nanoantenna. The immobilization mechanism, in brief, is that the d.c. electric field triggers the mobile ions in the electric double layer of the trapped object moving and then pushing the particle closer to the surface until the short-range attractive forces take effect to bind the object onto the nanoantenna surface.

Moreover, when the plasmonic nanoantenna is replaced with the nanohole array, the applied a.c. electric field is distorted by the nanoholes, resulting in both normal and tangential a.c. field components. The tangential component drives the diffuse charges in the electrical double layer at the interface between the nanohole array and the fluid, triggering localized a.c. electro-osmotic flow that has an opposite direction against the ETP flow (Fig. 12a) [109]. Recently, Ndukaife and co-workers have synergized the ETP flow and a.c. electro-osmotic flow to develop opto-thermo-electrohydrodynamic tweezers for the trapping and manipulation of sub-10 nm objects [43]. Since the strength of the a.c. electro-osmotic flow is increased faster than that the ETP flow at a lower a.c. frequency, the trapping distance of targeted objects relative to the laser position, i.e., the stagnation zone, can be adjusted by tuning the a.c. frequency (Fig. 12b). Thus, the object can be trapped several micrometers away from the laser focus, alleviating potential optical and thermal damage for safe biological sensing or single-molecule analysis. Furthermore, the trapped object can also be dynamically manipulated by translating the laser beam, like other optical-based tweezers (Fig. 12c).

8   Conclusion

By taking advantage of plasmonic optothermal effects, researchers have developed various heat-mediated optical tweezing techniques in recent years, enabling a versatile platform for precise manipulation of micro-and nano-objects. Thermophoretic tweezers trap the objects in the solution by exploiting the directed thermal migration of suspended objects under a laser heating-generated temperature gradient. Optothermoelectric tweezers present a more general approach to manipulate all kinds of colloids through the coordination of liquid thermoelectricity and surfactant modification of objects. To improve the trapping efficiency of plasmonic tweezers in dilute solution, various convection flows have been exploited to rapidly deliver particles toward the plasmonic hotspot. First, thermo-plasmonic convection can transport suspended particles mildly but usually requires large-area illumination for actuation, somehow sacrificing manipulation precision. Second, Marangoni convection enables more rapid delivery, but the target object might be directly printed on the substrate. In addition, the high temperature around the vapor bubble could cause damages to biological target objects. Last, ETP flow is newly developed in the last 5 years, which can transport suspended particles toward the trapping site rapidly and safely. However, an external electric field is required for ETP, which perplexes the experimental setup.

We expect the further developments of plasmon-enhanced optothermal manipulation in multiple directions to enhance the functions for the broader applications. Firstly, the capability of plasmon-enhanced optothermal manipulation in 3D will be improved. Due to the difficulty of optothermally constructing stable trapping potentials along the direction perpendicular to the plasmonic substrates, most single-particle manipulations have been limited to the in-plane directions along the substrates. Some methods have already been proposed to trap and manipulate particles in 3D via plasmon-induced optothermal fields. For instance, the plasmonic nanostructures were transferred onto optical fibers to realize 3D optothermal manipulation by simply controlling the position of the fiber tips [75]. Secondly it has been challenging to simultaneously achieve both high throughput and high precision for the plasmon-enhanced optothermal manipulation. To address the challenge, a spatial light modulator or digital micromirror device can be used to generate multiple laser beams for parallel manipulation of multiple particles [28]. Alternatively, the plasmonic nanostructures can be further elaborated to achieve multiple trapping potentials. Lastly, plasmon-enhanced optothermal manipulation has been mainly applied for particle assembly [76, 78] and in vitro sensing [39]. We envision that, with the further progress in the rational design of plasmonic nanostructures and heating source, in combination with additional external fields, the plasmon-enhanced optothermal trapping and tweezing will find more applications in materials science, biology, colloidal sciences, nanorobotics, and nanomanufacturing [110–112].

References

1. Ashkin, A., Dziedzic, J. M., Bjorkholm, J. E., & Chu, S. (1986). Observation of a single-beam gradient force optical trap for dielectric particles. *Optics Letters, 11*, 288–290.
2. Jauffred, L., Richardson, A. C., & Oddershede, L. B. (2008). Three-dimensional optical control of individual quantum dots. *Nano Letters, 8*, 3376–3380. https://doi.org/10.1021/nl801962f
3. Ashkin, A., Dziedzic, J. M., & Yamane, T. (1987). Optical trapping and manipulation of single cells using infrared laser beams. *Nature, 330*, 769–771. https://doi.org/10.1038/330769a0
4. Ashkin, A., & Dziedzic, J. M. (1987). Optical trapping and manipulation of viruses and bacteria. *Science, 235*, 1517. https://doi.org/10.1126/science.3547653
5. Urban, A. S., et al. (2014). Optical trapping and manipulation of Plasmonic nanoparticles: Fundamentals, applications, and perspectives. *Nanoscale, 6*, 4458–4474. https://doi.org/10.1039/C3NR06617G
6. Wright, W. H., Sonek, G. J., & Berns, M. W. (1993). Radiation trapping forces on microspheres with optical tweezers. *Applied Physics Letters, 63*, 715–717. https://doi.org/10.1063/1.109937
7. Preece, D., et al. (2011). Optical tweezers: Wideband microrheology. *Journal of Optics, 13*, 044022.
8. He, H., Heckenberg, N., & Rubinsztein-Dunlop, H. (1995). Optical particle trapping with higher-order doughnut beams produced using high efficiency computer generated holograms. *Journal of Modern Optics, 42*, 217–223.
9. Grigorenko, A. N., Roberts, N. W., Dickinson, M. R., & Zhang, Y. (2008). Nanometric optical tweezers based on nanostructured substrates. *Nature Photonics, 2*, 365–370. https://doi.org/10.1038/nphoton.2008.78
10. Juan, M. L., Righini, M., & Quidant, R. (2011). Plasmon nano-optical tweezers. *Nature Photonics, 5*, 349–356. https://doi.org/10.1038/nphoton.2011.56
11. Wang, K., Schonbrun, E., Steinvurzel, P., & Crozier, K. B. (2011). Trapping and rotating nanoparticles using a plasmonic nano-tweezer with an integrated heat sink. *Nature Communications, 2*, 469. https://doi.org/10.1038/ncomms1480
12. Yoo, D., et al. (2018). Low-power optical trapping of nanoparticles and proteins with resonant coaxial nanoaperture using 10 nm gap. *Nano Letters, 18*, 3637–3642.
13. Righini, M., Zelenina, A. S., Girard, C., & Quidant, R. (2007). Parallel and selective trapping in a patterned Plasmonic landscape. *Nature Physics, 3*, 477–480.
14. Roxworthy, B. J., et al. (2012). Application of plasmonic bowtie Nanoantenna arrays for optical trapping, stacking, and sorting. *Nano Letters, 12*, 796–801.
15. Berthelot, J., et al. (2014). Three-dimensional manipulation with scanning near-field optical Nanotweezers. *Nature Nanotechnology, 9*, 295–299.
16. Kotsifaki, D. G., Kandyla, M., & Lagoudakis, P. G. (2015). Near-field enhanced optical tweezers utilizing femtosecond-laser nanostructured substrates. *Applied Physics Letters, 107*, 211111.
17. Mundoor, H., et al. (2018). Tuning and switching a Plasmonic quantum dot "Sandwich" in a Nematic line defect. *ACS Nano, 12*, 2580–2590.
18. Huft, P. R., Kolbow, J. D., Thweatt, J. T., & Lindquist, N. C. (2017). Holographic Plasmonic Nanotweezers for dynamic trapping and manipulation. *Nano Letters, 17*, 7920–7925.

19. Kotsifaki, D. G., Kandyla, M., & Lagoudakis, P. G. (2016). Plasmon enhanced optical tweezers with gold-coated black silicon. *Scientific Reports, 6*, 26275. https://doi.org/10.1038/srep26275

20. Vigolo, D., Rusconi, R., Stone, H. A., & Piazza, R. (2010). Thermophoresis: Microfluidics characterization and separation. *Soft Matter, 6*, 3489–3493.

21. Kim, J.-D., & Lee, Y.-G. (2016). Graphene-based Plasmonic tweezers. *Carbon, 103*, 281–290.

22. Zhang, J., Liu, W., Zhu, Z., Yuan, X., & Qin, S. (2016). Towards nano-optical tweezers with graphene plasmons: Numerical investigation of trapping 10-nm particles with mid-infrared light. *Scientific Reports, 6*, 1–7.

23. Jiang, Q., Rogez, B., Claude, J.-B., Baffou, G., & Wenger, J. (2019). Temperature measurement in plasmonic nanoapertures used for optical trapping. *ACS Photonics, 6*, 1763–1773.

24. Jones, S., Andrén, D., Karpinski, P., & Käll, M. (2018). Photothermal heating of plasmonic nanoantennas: Influence on trapped particle dynamics and colloid distribution. *ACS Photonics, 5*, 2878–2887. https://doi.org/10.1021/acsphotonics.8b00231

25. Juan, M. L., Gordon, R., Pang, Y., Eftekhari, F., & Quidant, R. (2009). Self-induced Back-action optical trapping of dielectric nanoparticles. *Nature Physics, 5*, 915–919.

26. Righini, M., et al. (2009). Nano-optical trapping of Rayleigh particles and escherichia coli bacteria with resonant optical antennas. *Nano Letters, 9*, 3387–3391.

27. Kotnala, A., Kollipara, P. S., Li, J., & Zheng, Y. (2019). Overcoming diffusion-limited trapping in Nanoaperture tweezers using opto-thermal-induced flow. *Nano Letters, 20*, 768–779.

28. Lin, L., et al. (2018). Opto-thermoelectric Nanotweezers. *Nature Photonics, 12*, 195–201. https://doi.org/10.1038/s41566-018-0134-3

29. Braun, M., Bregulla, A. P., Günther, K., Mertig, M., & Cichos, F. (2015). Single molecules trapped by dynamic inhomogeneous temperature fields. *Nano Letters, 15*, 5499–5505.

30. Lin, L., Hill, E. H., Peng, X., & Zheng, Y. (2018). Optothermal manipulations of colloidal particles and living cells. *Accounts of Chemical Research, 51*, 1465–1474. https://doi.org/10.1021/acs.accounts.8b00102

31. Chen, Z., Kollipara, P. S., Ding, H., Pughazhendi, A., & Zheng, Y. (2021). Liquid Optothermoelectrics: Fundamentals and applications. *Langmuir, 37*, 1315–1336.

32. Chen, J., et al. (2020). Thermal Optofluidics: Principles and applications. *Advanced Optical Materials, 8*, 1900829. https://doi.org/10.1002/adom.201900829

33. Ndukaife, J. C., et al. (2016). Long-range and rapid transport of individual nano-objects by a hybrid Electrothermoplasmonic nanotweezer. *Nature Nanotechnology, 11*, 53–59. https://doi.org/10.1038/nnano.2015.248

34. Jauffred, L., Samadi, A., Klingberg, H., Bendix, P. M., & Oddershede, L. B. (2019). Plasmonic heating of nanostructures. *Chemical Reviews, 119*, 8087–8130.

35. Baffou, G., Quidant, R., & García de Abajo, F. J. (2010). Nanoscale control of optical heating in complex Plasmonic systems. *ACS Nano, 4*, 709–716.

36. Quinten, M. (2010). *Optical properties of nanoparticle systems: Mie and beyond*. Wiley.

37. Parsons, J., Burrows, C., Sambles, J., & Barnes, W. (2010). A comparison of techniques used to simulate the scattering of electromagnetic radiation by metallic nanostructures. *Journal of Modern Optics, 57*, 356–365.

38. Kang, Z., et al. (2015). Trapping and assembling of particles and live cells on large-scale random gold nano-Island substrates. *Scientific Reports, 5*, 9978. https://doi.org/10.1038/srep09978

39. Liu, Y., et al. (2018). Nanoradiator-mediated deterministic opto-thermoelectric manipulation. *ACS Nano, 12*, 10383–10392.

40. Ndukaife, J. C., et al. (2018). High-resolution large-ensemble nanoparticle trapping with multifunctional thermoplasmonic nanohole metasurface. *ACS Nano, 12*, 5376–5384. https://doi.org/10.1021/acsnano.8b00318

41. Lin, L., et al. (2018). Optothermoplasmonic nanolithography for on-demand patterning of 2d materials. *Advanced Functional Materials, 28*, 1803990. https://doi.org/10.1002/adfm.201803990

42. Sun, H., Yu, M., Wang, G., Sun, X., & Lian, J. (2012). Temperature-dependent morphology evolution and surface plasmon absorption of ultrathin Gold Island films. *The Journal of Physical Chemistry C, 116*, 9000–9008.

43. Hong, C., Yang, S., & Ndukaife, J. C. (2020). Stand-off trapping and manipulation of sub-10 nm objects and biomolecules using opto-thermo-electrohydrodynamic tweezers. *Nature Nanotechnology, 15*, 908–913. https://doi.org/10.1038/s41565-020-0760-z

44. Ebbesen, T. W., Lezec, H. J., Ghaemi, H., Thio, T., & Wolff, P. A. (1998). Extraordinary optical transmission through sub-wavelength hole arrays. *Nature, 391*, 667–669.

45. Popov, E., Neviere, M., Enoch, S., & Reinisch, R. (2000). Theory of light transmission through subwavelength periodic hole arrays. *Physical Review B, 62*, 16100.

46. Lin, L., et al. (2017). Thermophoretic tweezers for low-power and versatile manipulation of biological cells. *ACS Nano, 11*, 3147–3154.

47. Eslahian, K. A., Majee, A., Maskos, M., & Würger, A. (2014). Specific salt effects on thermophoresis of charged colloids. *Soft Matter, 10*, 1931–1936. https://doi.org/10.1039/C3SM52779D

48. Parola, A., & Piazza, R. (2004). Particle thermophoresis in liquids. *The European Physical Journal E, 15*, 255–263. https://doi.org/10.1140/epje/i2004-10065-5

49. Piazza, R., & Guarino, A. (2002). Soret effect in interacting micellar solutions. *Physical Review Letters, 88*, 208302. https://doi.org/10.1103/PhysRevLett.88.208302

50. Braibanti, M., Vigolo, D., & Piazza, R. (2008). Does Thermophoretic mobility depend on particle size? *Physical Review Letters, 100*, 108303.

51. Wiegand, S. (2004). Thermal diffusion in liquid mixtures and polymer solutions. *Journal of Physics: Condensed Matter, 16*, R357.

52. Duhr, S., Arduini, S., & Braun, D. (2004). Thermophoresis of DNA determined by microfluidic fluorescence. *The European Physical Journal E, 15*, 277–286.

53. Braun, M., & Cichos, F. (2013). Optically controlled Thermophoretic trapping of single nano-objects. *ACS Nano, 7*, 11200–11208. https://doi.org/10.1021/nn404980k

54. Fränzl, M., et al. (2019). Thermophoretic trap for single amyloid fibril and protein aggregation studies. *Nature Methods, 16*, 611–614.

55. Lin, L., et al. (2017). Interfacial-entropy-driven thermophoretic tweezers. *Lab on a Chip, 17*, 3061–3070.

56. Putnam, S. A., Cahill, D. G., & Wong, G. C. (2007). Temperature dependence of Thermodiffusion in aqueous suspensions of charged nanoparticles. *Langmuir, 23*, 9221–9228.

57. Hill, E. H., Li, J., Lin, L., Liu, Y., & Zheng, Y. (2018). Opto-thermophoretic attraction, trapping, and dynamic manipulation of lipid vesicles. *Langmuir, 34*, 13252–13262.

58. Peng, X., et al. (2018). Optothermophoretic manipulation of colloidal particles in nonionic liquids. *The Journal of Physical Chemistry C, 122*, 24226–24234. https://doi.org/10.1021/acs.jpcc.8b03828

59. Majee, A., & Würger, A. (2013). Thermocharge of a hot spot in an electrolyte solution. *Soft Matter, 9*, 2145–2153.

60. Reichl, M., Herzog, M., Götz, A., & Braun, D. (2014). Why charged molecules move across a temperature gradient: The role of Electric fields. *Physical Review Letters, 112*, 198101. https://doi.org/10.1103/PhysRevLett.112.198101

61. Würger, A. (2010). Thermal non-equilibrium transport in colloids. *Reports on Progress in Physics, 73*, 126601.

62. Ruckenstein, E. (1981). Can phoretic motions be treated as interfacial tension gradient driven phenomena? *Journal of Colloid and Interface Science, 83*, 77–81.

63. Bregulla, A. P., Würger, A., Günther, K., Mertig, M., & Cichos, F. (2016). Thermoosmotic flow in thin films. *Physical Review Letters, 116*, 188303. https://doi.org/10.1103/PhysRevLett.116.188303

64. Würger, A. (2008). Transport in charged colloids driven by thermoelectricity. *Physical Review Letters, 101*, 108302. https://doi.org/10.1103/PhysRevLett.101.108302
65. Würger, A. (2009). Temperature dependence of the soret motion in colloids. *Langmuir, 25*, 6696–6701.
66. Sehnem, A., et al. (2015). Temperature dependence of the soret coefficient of ionic colloids. *Physical Review E, 92*, 042311.
67. Morthomas, J., & Würger, A. (2008). Thermoelectric effect on charged colloids in the Hückel limit. *The European Physical Journal E, 27*, 425–434.
68. Majee, A., & Würger, A. (2011). Collective Thermoelectrophoresis of charged colloids. *Physical Review E, 83*, 061403.
69. Lüsebrink, D., & Ripoll, M. (2012). Collective thermodiffusion of colloidal suspensions. *The Journal of Chemical Physics, 137*, 194904.
70. Vigolo, D., Buzzaccaro, S., & Piazza, R. (2010). Thermophoresis and thermoelectricity in surfactant solutions. *Langmuir, 26*, 7792–7801. https://doi.org/10.1021/la904588s
71. Majee, A., & Würger, A. (2012). Charging of heated colloidal particles using the electrolyte seebeck effect. *Physical Review Letters, 108*, 118301. https://doi.org/10.1103/PhysRevLett.108.118301
72. Iacopini, S., & Piazza, R. (2003). Thermophoresis in protein solutions. *Europhysics Letters (EPL), 63*, 247–253. https://doi.org/10.1209/epl/i2003-00520-y
73. Ding, H., Kollipara, P. S., Lin, L., & Zheng, Y. (2020). Atomistic modeling and rational Design of Optothermal Tweezers for targeted applications. *Nano Research*. https://doi.org/10.1007/s12274-020-3087-z
74. Kollipara, P. S., Lin, L., & Zheng, Y. (2019). Thermo-electro-mechanics at individual particles in complex colloidal systems. *The Journal of Physical Chemistry C, 123*, 21639–21644.
75. Kotnala, A., & Zheng, Y. (2019). Opto-Thermophoretic fiber tweezers. *Nano, 8*, 475–485.
76. Lin, L., et al. (2019). All-optical reconfigurable chiral meta-molecules. *Materials Today, 25*, 10–20.
77. Lin, L., et al. (2016). Light-directed reversible assembly of plasmonic nanoparticles using plasmon-enhanced thermophoresis. *ACS Nano, 10*, 9659–9668. https://doi.org/10.1021/acsnano.6b05486
78. Lin, L., et al. (2017). Opto-thermophoretic assembly of colloidal matter. *Science Advances, 3*, e1700458.
79. Peng, X., Li, J., Lin, L., Liu, Y., & Zheng, Y. (2018). Opto-thermophoretic manipulation and construction of colloidal superstructures in photocurable hydrogels. *ACS Applied Nano materials, 1*, 3998–4004.
80. Lin, L., Peng, X., & Zheng, Y. (2017). Reconfigurable opto-thermoelectric printing of colloidal particles. *Chemical Communications, 53*, 7357–7360. https://doi.org/10.1039/C7CC03530F
81. Lin, L., Kollipara, P. S., & Zheng, Y. (2019). Digital manufacturing of advanced materials: Challenges and perspective. *Materials Today, 28*, 49–62. https://doi.org/10.1016/j.mattod.2019.05.022
82. Li, J., Hill, E. H., Lin, L., & Zheng, Y. (2019). Optical nanoprinting of colloidal particles and functional structures. *ACS Nano, 13*, 3783–3795. https://doi.org/10.1021/acsnano.9b01034
83. Li, J., Lin, L., Inoue, Y., & Zheng, Y. (2018). Opto-Thermophoretic tweezers and assembly. *Journal of Micro and Nano-Manufacturing, 6*. https://doi.org/10.1115/1.4041615
84. Pughazhendi, A., Chen, Z., Wu, Z., Li, J., & Zheng, Y. (2020). Opto-thermoelectric tweezers: Principles and applications. *Frontiers in Physics, 8*. https://doi.org/10.3389/fphy.2020.580014
85. Donner, J. S., Baffou, G., McCloskey, D., & Quidant, R. (2011). Plasmon-assisted optofluidics. *ACS Nano, 5*, 5457–5462.
86. Guyon, E., Hulin, J.-P., Petit, L., & Mitescu, C. D. (2001). *Physical hydrodynamics*. Oxford University Press.
87. Liu, Y., & Poon, A. W. (2010). Flow-assisted single-beam optothermal manipulation of microparticles. *Optics Express, 18*, 18483–18491. https://doi.org/10.1364/OE.18.018483

88. Chen, J., Kang, Z., Kong, S. K., & Ho, H.-P. (2015). Plasmonic random nanostructures on fiber tip for trapping live cells and colloidal particles. *Optics Letters, 40*, 3926–3929. https://doi.org/10.1364/OL.40.003926

89. Cong, H., et al. (2019). Target trapping and in situ single-cell genetic marker detection with a focused optical beam. *Biosensors and Bioelectronics, 133*, 236–242.

90. Jin, C. M., Lee, W., Kim, D., Kang, T., & Choi, I. (2018). Photothermal convection lithography for rapid and direct assembly of colloidal plasmonic nanoparticles on generic substrates. *Small, 14*, 1803055. https://doi.org/10.1002/smll.201803055

91. Scriven, L., & Sternling, C. (1960). The Marangoni effects. *Nature, 187*, 186–188.

92. Li, X., et al. (2019). Plasmonic bubble nucleation and growth in water: Effect of dissolved air. *The Journal of Physical Chemistry C, 123*, 23586–23593. https://doi.org/10.1021/acs.jpcc.9b05374

93. Wang, Y., et al. (2018). Giant and explosive Plasmonic bubbles by delayed nucleation. *Proceedings of the National Academy of Sciences, 115*, 7676–7681. https://doi.org/10.1073/pnas.1805912115

94. Girot, A., et al. (2016). Motion of optically heated spheres at the water–Air interface. *Langmuir, 32*, 2687–2697.

95. Zhao, C., et al. (2014). Theory and experiment on particle trapping and manipulation via Optothermally generated bubbles. *Lab on a Chip, 14*, 384–391. https://doi.org/10.1039/C3LC50748C

96. Kim, Y., Ding, H., & Zheng, Y. (2020). Enhancing surface capture and sensing of proteins with low-power Optothermal bubbles in a biphasic liquid. *Nano Letters, 20*, 7020–7027. https://doi.org/10.1021/acs.nanolett.0c01969

97. Miniewicz, A., Quintard, C., Orlikowska, H., & Bartkiewicz, S. (2017). On the origin of the driving force in the Marangoni propelled gas bubble trapping mechanism. *Physical Chemistry Chemical Physics, 19*, 18695–18703.

98. Rajeeva, B. B., et al. (2019). Accumulation-driven unified spatiotemporal synthesis and structuring of immiscible metallic nanoalloys. *Matter, 1*, 1606–1617. https://doi.org/10.1016/j.matt.2019.10.017

99. Bangalore Rajeeva, B., et al. (2017). High-resolution bubble printing of quantum dots. *ACS Applied Materials & Interfaces, 9*, 16725–16733. https://doi.org/10.1021/acsami.7b04881

100. Rajeeva, B. B., et al. (2017). Patterning and fluorescence tuning of quantum dots with haptic-interfaced bubble printing. *Journal of Materials Chemistry C, 5*, 5693–5699. https://doi.org/10.1039/C7TC00454K

101. Rajeeva, B. B., et al. (2018). "Point-and-shoot" synthesis of metallic ring arrays and surface-enhanced optical spectroscopy. *Advanced Optical Materials, 6*, 1701213. https://doi.org/10.1002/adom.201701213

102. Lin, L., et al. (2016). Bubble-pen lithography. *Nano Letters, 16*, 701–708. https://doi.org/10.1021/acs.nanolett.5b04524

103. Hu, W., Fan, Q., & Ohta, A. T. (2013). An opto-thermocapillary cell micromanipulator. *Lab on a Chip, 13*, 2285–2291. https://doi.org/10.1039/C3LC50389E

104. Chikazawa, J.-I., Uwada, T., Furube, A., & Hashimoto, S. (2019). Flow-induced transport via optical heating of a single gold nanoparticle. *The Journal of Physical Chemistry C, 123*, 4512–4522. https://doi.org/10.1021/acs.jpcc.8b11575

105. Dai, L., Ge, Z., Jiao, N., & Liu, L. (2019). 2d to 3d manipulation and assembly of microstructures using Optothermally generated surface bubble microrobots. *Small, 15*, 1902815. https://doi.org/10.1002/smll.201902815

106. Stratton, J. A. (2007). *Electromagnetic theory* (Vol. 33). Wiley.

107. Melcher, J., & Electric, R. (1974). Fields and moving media. *IEEE Transactions on Education, 17*, 100–110.

108. Roxworthy, B. J., Bhuiya, A. M., Vanka, S. P., & Toussaint, K. C. (2014). Understanding and controlling Plasmon-induced convection. *Nature Communications, 5*, 3173. https://doi.org/10.1038/ncomms4173

109. Squires, T. M., & Bazant, M. Z. (2004). Induced-charge electro-osmosis. *Journal of Fluid Mechanics, 509*, 217–252.
110. Li, J., et al. (2021). Tunable chiral optics in all-solid-phase reconfigurable dielectric nanostructures. *Nano Letters, 21*, 973–979. https://doi.org/10.1021/acs.nanolett.0c03957
111. Li, J., et al. (2019). Optical nanomanipulation on solid substrates via optothermally-gated photon nudging. *Nature Communications, 10*, 5672. https://doi.org/10.1038/s41467-019-13676-3
112. Kotnala, A., & Zheng, Y. (2019). Digital assembly of colloidal particles for nanoscale manufacturing. *Particle & Particle Systems Characterization, 36*, 1900152. https://doi.org/10.1002/ppsc.201900152